Single-cell analysis of bovine muscle-derived cell types for cultured meat production

Tobias Messmer[1,2], Richard GJ Dohmen[1,2], Lieke Schaeken[1], Lea Melzener[1,2], Rui Hueber[1], Mary Godec[1], Mark J Post[1,2], Joshua E Flack*[1]

Affiliation: [1]Mosa Meat, [2] Maastricht University

Keywords: single-cell RNA sequencing, cultured meat, cell purification, muscle stem cells, satellite cell heterogeneity

Abstract

'Cultured' meat technologies leverage the proliferation and differentiation of animal-derived stem cells *ex vivo* to produce edible tissues for human consumption in a sustainable fashion. However, skeletal muscle is a dynamic and highly complex tissue, involving the interplay of numerous mono- and multinucleated cells, including muscle fibres, satellite cells (SCs) and fibro-adipogenic progenitors (FAPs), and recreation of the tissue *in vitro* thus requires the characterisation and manipulation of a broad range of cell types. Here, we use a single-cell RNA sequencing approach to characterise cellular heterogeneity within bovine muscle and muscle-derived cell cultures over time. Using this data, we identify numerous distinct cell type, and develop robust protocols for the easy purification and proliferation of several of these populations. We note overgrowth of undesirable cell types within heterogeneous proliferative cultures as a barrier to efficient cultured meat production, and use transcriptomics to identify conditions that favour the growth of SCs in the context of serum-free medium. Combining RNA velocities computed in silico with time-resolved flow cytometric analysis, we characterise dynamic subpopulations and transitions between active, quiescent, and committed states of SCs, and demonstrate methods for modulation of these states during long-term proliferative cultures. This work provides an important reference for advancing our knowledge of bovine skeletal muscle biology, and its application in the development of cultured meat technologies.

Introduction

'Cultured' or 'cultivated' meat is an emergent technology that leverages in vitro proliferation and differentiation of stem cells to produce edible tissues that mimic conventional meat[1,2]. Whilst there are numerous potential advantages to this technology, including reduced greenhouse gas emissions and improved animal welfare[3], many technical challenges remain, such as the removal of animal-derived components, scaling of culture volumes, and cost reduction[4,5]. Moreover, consumer acceptance will be reliant on the taste and texture of cultured meat products closely replicating those of the conventionally-reared equivalent[6,7].

Meat is composed primarily of skeletal muscle, a complex tissue whose function requires the interplay of numerous mono- and multinucleated cell types, including muscle fibres, satellite cells (SCs) and fibro-adipogenic progenitors (FAPs), as well as vascular, nervous and connective tissue[8,9]. Whilst most cultured meat products currently being pursued consist of unstructured muscle fibres, with or without fat tissue, accurate recreation of the entire tissue requires the identification, purification, proliferation and characterisation of a broad range of cell types[10,11]. Descriptions of the composition of human and murine skeletal muscle at the cellular level are now available[12–16], but a similarly detailed understanding of muscle biology in agriculturally relevant species, such as cattle, is currently lacking. Furthermore, the extent to which complex muscle-derived cell behaviours and interactions are recapitulated during in vitro culture is unclear[17,18], limiting the progress of cultured meat development.

Here, we used droplet-based single-cell RNA sequencing (scRNA-seq) to profile bovine skeletal muscle, and muscle-derived cell cultures, in a time-resolved fashion across the process of cultured meat production. We use the resultant dataset to gain insight into transcriptional heterogeneity between and within cell types, and to inform various steps of cultured meat bioprocess design.

Results

scRNA-seq identifies 11 distinct cell types in bovine muscle

In order to investigate heterogeneity between and within bovine muscle-derived cell types, we used the 10x Chromium platform for scRNA-seq to study gene expression at five timepoints in a primary adult stem cell-based cultured meat production process (Fig. 1a, Supplementary Table 1). A total of 36129 single-cell transcriptomes, with an average expression of 3815 genes and 21131 transcripts per cell, were analysed across 10 donor cattle and assembled into a single dataset (Supplementary Fig. 1). Using UMAP dimensionality reduction, based on the first 30 principal components (Fig. 1b), cells from Timepoints 1 (muscle tissue) and 2 (passage 0, after 72 h in vitro culture) clustered separately from each other, and from Timepoints 3 to 5 (after passages 2, 5 and 8 respectively), indicating significant transcriptomic changes between timepoints and within cell types during the proliferative process.

Within enzymatically digested bovine muscle tissue (Timepoint 1), we identified 11 defined populations of mononuclear cells with distinct gene expression profiles (Fig. 1c; Supplementary Table 2), which were present in varying proportions in all donor animals (Supplementary Fig. 2a). Based on differential gene expression, these clusters were assigned to cell types previously characterised in other species[12,13,19], namely fibro-adipogenic progenitors (FAPs), satellite cells (SCs), vascular and lymphatic endothelial cells (ECs; vascular, VECs; lymphatic, LECs, Supplementary Fig. 2b), smooth muscle and mesenchymal cells (SMMCs), monocytes/macrophages (MΦ), neutrophils, lymphocytes (B/T/NK cells), glial cells, tenocytes and myocytes (Fig. 1d, Supplemental Fig. 2d). The expression of canonical genes in each of these populations in analogous studies indicated their conservation between mouse and cattle (Fig. 1e, Supplemental Fig. 2e)[14].

Cell types can be identified in vitro by unique surface marker expression

In order to identify proliferative muscle tissue-derived cell types that might be used for cultured meat production, we analysed the adherent cell fraction after 72 h (Timepoint 2) culture in serum-free growth medium (SFGM, Supplementary Table 3). We discerned 7 populations present in these cultures, which were separated from the same populations in Timepoint 1 by UMAP, indicating stark transcriptional changes during the transition to in vitro culture (Fig. 2a). GO terms corresponding to differentially expressed genes (independent of cell type) between Timepoints 1 and 2 (Fig. 2b) suggest that these transcriptional switches relate to decreased interaction with the extracellular matrix (ECM) and increased protein production, concomitant with increased cellular proliferation in the in vitro environment.

Comparison of Timepoints 1 and 2 enabled the assigning of cell identities to individual clusters (Fig. 2c), indicating that of the 11 populations identified in Timepoint 1, only myocytes, tenocytes, neutrophils and lymphocytes did not persist in short-term serum-free culture. Conversely, FAPs, SCs, SMMCs, ECs, glial cells and monocytes/macrophages remained present in cultures from all genotypes (donor animals) sequenced (Supplementary Figs. 3a, b). These same cell types were identified when culturing cells in growth medium (GM) containing 20% foetal bovine serum (FBS; Supplementary Fig. 3c, Supplementary Table 3), indicating that our SFGM formulation was able to support culture of muscle-derived cells as robustly as traditional serum-containing media.

Analysis of differentially expressed genes yielded highly and exclusively expressed markers for each population (Fig. 2d)[10,20] that have previously been described in mouse and human[12–14,21]. Filtering these lists for genes encoding plasma membrane-localised proteins facilitated the identification of candidate cell surface markers for separation of populations by flow cytometry (Fig. 2e). Staining of muscle tissue-derived cells 72 h post-isolation for JAM-1 (*F11R*), CD45 (*PTPRC*), ITGA7 and ITGA5 confirmed the suitability of this quartet of markers as a FACS panel (Fig. 2f, Supplementary Fig. 3d).

105 **Four principal muscle-derived cell types can be proliferated in vitro**

106

107 In order to characterise their in vitro phenotypes in more detail, we sorted muscle-derived cells
108 into FAPs, SCs, ECs and SMMCs using the FACS panel previously described (Fig. 2). The
109 purified populations exhibited markedly different morphologies; whilst FAPs had a spindle-like
110 morphology and SCs were more spherical, ECs and SMMCs appeared flatter and larger (Fig. 3a).
111 Flow cytometric analysis post-FACS using the same antibody panel confirmed high sorting
112 purities for all populations (Fig. 3b). In addition, immunofluorescent staining for canonical markers
113 PDGFRα, Pax7, TEK (also known as Tie2), and Calponin-1 (CNN1) further verified the identity of
114 FAPs, SCs, ECs, and SMMCs respectively (Fig. 3c).

115

116 Long-term proliferation of each of these populations was supported in SFGM (FAPs, SCs) or
117 BioAMF-3 medium (ECs, SMMCs), with each culture undergoing at least 15 population doublings
118 (PDs) over a period of at least 6 passages (Fig. 3d). Proliferation rates varied between cell types
119 (for example, from 0.46 (ECs) to 1.0 PDs/day (SMMCs) at early passage), and tended to decrease
120 over time (Fig. 3e).

121 **Optimised culture conditions prevent SC overgrowth by FAPs**

122

123 We next aimed to understand heterogeneity within FACS-purified SC cultures during long-term
124 proliferation. Surprisingly, we found that cells in these cultures clustered into two distinct
125 populations, marked by differential expression of *ITGA7* (Fig. 4a). *ITGA7*- cells expressed FAP
126 marker genes such as *ITGA5* (Supplemental Fig. 4a, Fig. 2), suggesting that these cells were
127 FAPs that were inaccurately sorted into, and remained prevalent within, SC cultures.
128 Quantification of these cell types showed that the proportion of FAPs increased over time,
129 indicating that our standard culture conditions favoured long-term proliferation of FAPs over SCs
130 (Fig. 4b, Supplemental Fig. 4b). The percentage of contaminating FAPs correlated negatively with
131 myogenic differentiation, as determined by fusion index (Figs. 4c, d), emphasising the importance
132 of eliminating overgrowth by non-SCs for cultured muscle production.

133

134 We therefore sought to adapt the long-term culture conditions, with the aim of preventing FAPs
135 from overgrowing SCs. To inform our approach, we filtered the scRNA-seq data for differentially
136 expressed genes between SCs and FAPs encoding receptors that interact with proteins
137 commonly used as surface coatings or growth factors, revealing a number of interesting
138 candidates (Fig. 4e, f). Sorting SCs using an ITGA7+/ITGA5- strategy significantly decreased FAP
139 contamination as compared to a CD29+/NCAM1+ sorting strategy (used in previous studies[22]),
140 reducing FAP overgrowth after multiple passages (Figs. 4g, h). Culturing SCs contaminated with
141 FAPs on different coatings, we observed that within 3 passages, SC purity was reduced on
142 collagen I and fibronectin (FN; interacting with ITGA5) but remained high on laminin-521 (LN-521;
143 interacting with ITGA7; Fig. 4i). We further adapted SFGM by adding triiodothyronine (T3, 30 nM,
144 ligand for THRA), increasing the concentration of HGF (ligand for c-Met) and removing PDGF-BB
145 (ligand for PDGFRα; Fig. 4j). Each individual adaptation reduced FAP overgrowth over 3
146 passages, whilst the combination of all three showed no significant reduction in SC proportion
147 over the course of the experiment, and was thus labelled 'improved SFGM' (i-SFGM).

148 **SCs transition between three dynamic states**

149

150 To further investigate SC heterogeneity in vitro, we filtered out FAPs and reanalysed the
151 remaining single-cell transcriptomes at passage 2 (Timepoint 3). Reclustering identified three
152 subpopulations within SCs, with distinct gene expression profiles suggestive of quiescent,
153 activated, and committed states (similar to those previously observed in murine SCs[14]; Figs. 5a,
154 b). Genes encoding proteins related to focal adhesion and ECM organisation were upregulated
155 in the quiescent state, cell cycle and replication in the activated state, and myogenic differentiation
156 the committed state (Fig. 5c, Supplementary Fig. 5a). These cell states were also observed at
157 passages 5 and 8, but in different ratios (Supplementary Figs. 5b, c), suggesting the possibility of
158 transitioning between states.

159

160 We next established protocols to measure these states in vitro, through analysis of CD151
161 (upregulated in quiescent SCs[14]) and desmin (upregulated in committed SCs) via flow cytometry
162 (Fig. 5d, Supplementary Fig. 5d). Combining this panel with EdU-staining, we confirmed
163 increased cell cycle activity in activated as compared to quiescent SCs (Fig. 5e; Supplementary
164 Fig. 5e). Investigating the dynamics of these subpopulations during a single passage, we found
165 dynamic conversion between quiescent (CD151+) and activated (CD151-) states, with an initial
166 increase in quiescent SCs followed by a rapid decline and a renewed increase as cells approach
167 confluence (Fig. 5f). The proportion of cells in the committed state remained stable throughout
168 the first 72 h, increasing after 96 h. Investigating over multiple passages revealed that this
169 interchangeability decreased over time (Supplementary Fig. 5f). We observed that i-SFGM
170 increased the proportion of activated SCs compared to SFGM, both within a single passage (Fig.
171 5f) and over the course of multiple passages (Supplementary Fig. 5f). In addition to transitions
172 between cell states changing over the course of cell aging, transcriptional changes related to
173 increased ECM remodelling and decreased translation were also observed *within* states over time
174 (Supplementary Fig. 6).

175

176 Finally, we performed RNA velocity analysis of SCs at passage 2, in order to investigate these
177 cell state transitions in silico. RNA velocity averaged across all genes indicated transitions from
178 the activated to the quiescent state or committed states (Fig. 5g), whilst an increase in expression
179 of cell cycle genes within a subset of quiescent cells suggested they are able to return to the
180 activated state (Fig. 5h). Taken together with in vitro data, this suggests a dynamic, reversible

181 transition between activated and quiescent states, whilst activated cells can also differentiate
182 towards committed myocytes as SCs become confluent (Fig. 5i).

183 # Discussion

184 The complexity of muscle tissue arises from the interplay of multiple cell types[8,9]. Here, we have
185 presented an annotated scRNA-seq dataset comprising over 36,000 muscle cellular
186 transcriptomes, from 10 donor cattle, across five timepoints during a cultured beef production
187 process. This dataset gives significant insight into the cellular heterogeneity present in bovine
188 skeletal muscle for the first time, including comprehensive analysis of 11 defined cell types (Fig.
189 1). Our analysis showed notable similarity between bovine muscle and analogous approaches
190 employed for more well-studied species, with expression of canonical genes for distinct cell types
191 largely conserved between cattle, human and mouse. Comparison of bovine muscle with the
192 corresponding cell cultures shed light on transcriptional changes that occur during the transition
193 to in vitro culture. Notably, genes related to protein synthesis were strongly upregulated
194 (suggesting cell activation), whilst those relating to ECM were downregulated, highlighting the
195 pivotal role of cell-matrix interactions in the muscle niche. However, despite the absence of
196 signalling from the microenvironment, the expression of most canonical marker genes was
197 conserved in vitro (Fig. 2), suggesting that muscle-derived cell cultures are able to recapitulate in
198 vivo behaviour to a large extent.
199
200 Differential expression analysis allowed us to identify surface marker panels for physical
201 separation of multiple cell types, including SCs, FAPs, ECs and SMMCs (together representing
202 over 80% of mononucleated cells). Notably, inclusion of ITGA5 in the panel offered significant
203 purity improvements over previous protocols, as this integrin serves as a negative selection
204 marker for SCs, whilst ITGB1/CD29 (previously used as a SC marker[22,23]) is highly expressed by
205 both SCs and FAPs. Whilst we were able to proliferate each of these cell types for multiple
206 passages (Fig. 3), further work is needed to assess the potential of ECs and SMMCs, with respect
207 to their long-term proliferation in the absence of FBS and their capacity to promote myogenesis
208 or adipogenesis, for example in co-culture systems[12,24]. Other low-abundance cell types, such as
209 macrophages, could also offer benefits in terms of tissue remodelling and angiogenesis for
210 structured cultured meat products[25,26].
211
212 Cultured meat production requires an extensive proliferation phase, with many PDs, to achieve
213 required cell yields[5]. This prompts several issues, including reduced growth rates, loss of
214 differentiation capacity, and the possibility of overgrowth of undesired cell types. Transcriptomic
215 analysis indeed revealed that sorted SCs were rapidly overgrown by a small proportion of

contaminating FAPs, indicating variable growth dynamics in our initial culture conditions that favour FAP proliferation (Fig. 4). Whilst high levels of animal-derived sera have traditionally been used to control fibroblastic overgrowth in SC cultures[27], this phenomenon is poorly understood, and in any case is unsuited for cultured meat applications. We used differential expression analysis to inform several improvements to the SC culture conditions, including the switch to an ECM mimic that corresponds to the integrin expression profile of SCs (laminin is known to interact with ITGA7/ITGB1 dimers[28]), and the addition of growth factors, such as HGF, whose receptor expression is specific to SCs[29,30]. Our dataset will also provide insights into design of selective media for other cell types, such as ECs, which is likely complicated by their slow proliferation. Detailed metabolic profiling, which was beyond the scope of this study, could help to further inform the design of feeding strategies that afford efficient and selective growth of desired cell types[31]. It should be noted that our experiments are conducted at lab scale, and that proliferation in bioreactor systems used for upscaled cultured meat production will introduce additional stresses, that could act differentially across cell types[32]. Further cost reduction will also be required, and our dataset can assist in the replacement of growth and attachment factors with peptide alternatives with retained (or superior) cell type selectivities.

Our transcriptomic analysis also revealed remarkable heterogeneity *within* cell types, notably between distinct subpopulations of SCs, that points towards a dynamic equilibrium of quiescent, active and committed states (Fig. 5). Different SC states have previously been proposed, both from dissociated muscle samples[15,33–35] and in vitro cultures[16,36,37], although without clear consensus. We identified CD151 (previously observed in human skeletal muscle[13]) as a cell-surface marker for the 'quiescent' cluster, although the extent to which the quiescent phenotype we observed in vitro reflects physiological SC behaviour during embryonic development or wound healing remains unclear. We did not distinguish such states in our bovine muscle samples, perhaps because the majority of cells are activated during tissue dissociation[33]. RNA velocity analysis suggests a model in which only activated SCs are able to differentiate, which is congruent with a physiological model of wound healing in which activated SCs either differentiate to form muscle fibres, or return to a quiescent state in order to preserve the ability of the tissue to respond to future regenerative stimuli. However, higher resolution velocity analysis of SCs would be informative, given that we only sampled a snapshot within each passage (when cells were approaching confluency). Indeed, the role that confluency plays in the promotion of differentiation, and the extent to which premature differentiation might negatively affect a proliferative culture, requires further study in the context of a cultured meat bioprocess design. Similarly, whilst

250 increased culture length clearly affects the transitions of SCs between states, it is important to
251 note that we also observed substantial transcriptomic differences between equivalent states at
252 different timepoints (Supplementary Fig. 6), indicating that cellular aging cannot be understood
253 solely in terms of subpopulation ratio changes. Indeed, our data supports the hypothesis that a
254 reduced rate of switching between states could be a characteristic of SC aging or senescence[38,39].
255 Future transcriptomic experiments, including single-nuclei approaches, could illuminate the
256 formation of cultured muscle tissues during the differentiation of SCs. Furthermore, although not
257 specified in this study, it is likely that similar cellular heterogeneity is present in other cell types,
258 including FAPs, where adipogenic and fibroblastic fate decisions could be critical for cultured fat
259 production[40,41].
260
261 In conclusion, scRNA-seq is a powerful approach to study cell heterogeneity in the context of
262 cultured meat production. Our dataset offers a number of important insights for cell purification
263 and proliferation steps, has led to the development of refined medium conditions, and represents
264 a useful resource for further analysis and improvement of cultured meat bioprocesses.

Material & Methods

Cell isolation

Cells were isolated from semitendinosus muscles of 10 Belgian Blue cattle (Supplementary Table 1) by collagenase digestion (CLSAFA, Worthington; 1 h; 37 °C), filtration with 100 µm cell strainers, red blood lysis using a Ammonium-Chloride-Potassium (ACK) lysis buffer, and final filtration with 40 µm cell strainers. Cells from each donor animal were plated as separate cultures in serum-free growth medium[42] (SFGM, Supplementary Table 3) on fibronectin-coated (4 µg cm^{-2} bovine fibronectin; F1141, Sigma-Aldrich) tissue culture vessels for 72 h prior to FACS, or (where denoted) in growth medium (GM) containing 20% foetal bovine serum (heat-inactivated FBS; 10500-064, Gibco).

Cell culture

Tissue culture vessels were coated with fibronectin for unsorted cells, ECs, and SMMCs, laminin-521 (0.5 µg cm^{-2}, LN521-05, Biolamina) for SCs, or collagen I (0.6 µg cm^{-2}, bovine skin collagen; C2124, Sigma-Aldrich) for FAPs for 1 h prior to plating. Unsorted cells, SCs and FAPs were cultured in SFGM (except where otherwise noted), and passaged every 3-4 days upon reaching confluency. ECs and SMMCs were cultured in BioAMF-3 (01-196-1A, Sartorius).

To assess long-term proliferation, cells were cultured as described above for each cell type. Cells were harvested upon approaching confluence, counted, reseeded at $5x10^3$ cm^{-2} and purity assessed at each passage via flow cytometry.

Single cell RNA-sequencing

Cell harvesting

Five timepoints throughout long-term in vitro culture were selected for single-cell RNA sequencing (scRNA-seq), for each of which cells from all genotypes (donor animals) were pooled in equal ratios and washed with 1% BSA in PBS prior to injection. Timepoints 1 to 5 corresponded to unsorted cells directly after isolation ('Muscle') and after 72 h ('passage 0'), and to cultured cells (unsorted cells, SCs and FAPs) at passages 2, 5, and 8 respectively (Fig. 1a, Supplementary Table 1).

Library preparation and sequencing

298 25000 cells were injected for each timepoint into Chromium Single Cell Controller, emulsified with
299 bar-coded gel beads and libraries were constructed following the protocol of the Chromium
300 NextGEM Single Cell 3' Kit V3.1 (10x Genomics). Quality control of the DNA library was performed
301 on Qiaxcel (QIAgen) and quantified by qPCR using the KAPA SYBR Fast qPCR Master Mix
302 (Illumina). Paired- end single cell 3' gene expression libraries were sequenced on a Novaseq
303 6000 System (Illumina) using a NovaSeq S1 flow-cell to a depth of at least 3.5 x 10^8
304 reads/timepoint.
305
306 *Data processing and demultiplexing*
307 Raw base call files were demultiplexed using the cellranger mkfastq function (CellRanger 6.0.1).
308 Reads were aligned to Bos Taurus genome (build ARS-UCD1.2) with Ensembl annotations
309 (release 101), using CellRanger count function. Default filtering parameters of CellRanger were
310 applied to obtain a gene expression matrix. Genotypes were deconvolved and assigned to
311 individual cells using demuxlet[43], based on VCF files previously generated by genotyping of each
312 donor animal with a BovineSNP50 v3 DNA Analysis BeadChip (Illumina).
313
314 *Quality control and normalisation*
315 Across the five timepoints, 36129 cells (90.8%) passed quality control (within 3 median absolute
316 deviations of the median for expressed genes, total counts and percentage mitochondrial genes;
317 Supplementary Fig. 1). Counts for each timepoint were normalised using the sctransform function
318 of Seurat with default parameters[44,45], regressing out percentage of mitochondrial genes, library
319 size, number of genes, and cell cycle effects.
320
321 *Dimensionality reduction and differential gene expression analysis*
322 Cells were clustered using the FindNeighbors() and FindClusters() functions based on the first 50
323 principal components and with a resolution of 0.1 respectively. Dimensionality was reduced by
324 uniform manifold approximation and projection (UMAP)[46] using the first 30 principal components
325 as input, 50 neighbouring points and a minimal distance of 0.1).
326
327 Differentially expressed (DE) genes were computed for clusters identified in each timepoint by
328 using the FindAllMarkers(), or between denoted conditions using FindMarkers(), with a $\log_2$ fold-
329 change (log-FC) threshold of 1, a false discovery rate (FDR) of 0.05, and expressed in at least
330 50% of cells. For Timepoint 1, cell types were assigned to each cluster based on DE genes and
331 on predicted phenotypes from FindTransferAnchors()[47] using analogous murine scRNA-seq data

332 (GSE143437[14]). ECs were further characterised by their expression of signatures derived from
333 the Descartes human genes expression atlas[19] using the AddModuleScore function. For
334 Timepoint 2, surface markers amongst the DE genes were identified by filtering for genes coding
335 for proteins located in the plasma membrane[48]. GO terms for biological processes (2021) were
336 computed using enrichR[49]. For the analysis of SC cultures, Timepoints 3 to 5 were filtered for
337 genotypes 5, 6, and 10 (Fig. 4), whilst for analysis of SC states these were further filtered by
338 removal of *ITGA5*+ FAP clusters (Fig. 5).
339
340 *RNA velocity analysis*
341 RNA velocities were computed for SCs at Timepoint 3 by generating separate count matrices for
342 spliced and unspliced transcripts using velocyto. The resulting loom files were analysed using
343 scVelo in Python 3.9.12. Transcription kinetics for selected genes were computed, as well as RNA
344 velocity vectors (based on the scVelo dynamical model) across all genes[50,51].
345
346 **Flow cytometry**
347 For cell type identification, unsorted cells were stained for ITGA5, ITGA7, JAM-1 and CD45 (Fig.
348 3, Supplementary Table 4) for 15 min prior to analysis on a MACSQuant10 Flow Analyzer (Miltenyi
349 Biotec). To determine proportions of SCs and FAPs (Fig. 4), cells were stained for ITGA7 and
350 ITGA5. For analysis of SC states (Fig. 5), cells were stained for CD151 prior to fixation (PFA),
351 permeabilisation (10% saponin), and staining for desmin. Samples were subsequently washed
352 and stained with α-mouse-PE secondary antibodies prior to analysis.
353
354 **Fluorescent-activated cell sorting (FACS)**
355 Cells were purified by FACS 72 h post-isolation on a MACSQuant Tyto Cell Sorter (Miltenyi
356 Biotec) following antibody staining as described above. SCs, FAPs, SMMCs and ECs were gated
357 as described in Fig. 2. Where noted, cells were gated for NCAM1+/CD29+ (Fig. 4g).
358
359 **Immunofluorescent staining**
360 After formaldehyde fixation, cells were permeabilised (0.5% Triton X-100), blocked (2% bovine
361 serum albumin (BSA)) and stained with PDGFRα, Pax7, TEK, and CNN1 (for phenotype
362 confirmation; Fig. 3c) or desmin (for fusion index; Fig. 4c) primary antibodies (see Supplementary
363 Table 4). After washing, cells were incubated with AF488-conjugated secondary antibodies and
364 Hoechst 33342 (Thermo Fisher) prior to imaging on an ImageXpress Pico Automated Cell
365 Imaging System (Molecular Devices).

366

367 **Myogenic differentiation assay**

368 Mixed cultures containing SCs and FAPs in varying proportions were seeded on 0.5% Matrigel-
369 coated vessels at a density of $5x10^4$ cm^{-2} in SFGM for 24 h, before switching to serum-free
370 differentiation media (SFDM). After 72 h in SFDM, cells were fixed with 4% formaldehyde, stained
371 for desmin and imaged as previously described. To calculate fusion indices, number of nuclei
372 within desmin-stained areas were divided by total nuclei.

373

374 **Cell cycle analysis**

375 For flow cytometric cell cycle analysis, SCs were incubated with EdU for 90 min prior to
376 trypsinisation. Following α-CD151-APC staining, Click-iT reaction was performed using the Click-
377 iT EdU Alexa Fluor 488 Flow Cytometry Assay Kit (C10420, Thermo Fisher) according to the
378 supplier's protocol, followed by α-desmin staining as previously described. Finally, the cells were
379 gated into quiescent ($DES^-/CD151^+$) and activated ($DES^-/CD151^-$) and within these, into EdU^+ (S-
380 Phase), $DAPI^{low}/EdU^-$ (G0/1-Phase) and $DAPI^{high}/EdU^-$ (G2-Phase), as shown in Supplementary
381 Fig. 5d.

382

383 **Statistical analyses**

384 Statistical analyses were performed using Prism 9 (Graphpad). Pearson correlation of fusion
385 indices with percentages of ITGA7+ cells was computed assuming a normal distribution (Fig. 4d).
386 For comparisons of culture conditions (Figs. 4h-j) and the analysis of cell cycle states in SCs (Fig.
387 5e), two-way ANOVAs were performed including post-hoc Tukey's multiple comparison test.
388 Sample replicates consisted of cells from the same donor animal, cultured in separate vessels.

389

390 **Data availability**

391 scRNA-seq data is deposited in the NCBI Gene Expression Omnibus database (accession code
392 GSE211428).

393

394 **Code availability**

395 Code for scRNA-seq analysis (including RNA velocity calculations) are available from the authors
396 on request.

397 # Bibliography

398 1. Post, M. J. Cultured beef: medical technology to produce food. *J. Sci. Food Agric.* **94**, 1039–
399 1041 (2014).
400 2. Datar, I. & Betti, M. Possibilities for an in vitro meat production system. *Innov. Food Sci.*
401 *Emerg. Technol.* **11**, 13–22 (2010).
402 3. Parodi, A. *et al.* The potential of future foods for sustainable and healthy diets. *Nat. Sustain.*
403 **1**, 782–789 (2018).
404 4. Post, M. *et al.* Scientific, sustainability and regulatory challenges of cultured meat. *Nat. Food*
405 **1**, 403–415 (2020).
406 5. Melzener, L., Verzijden, K. E., Buijs, A. J., Post, M. J. & Flack, J. E. Cultured beef: from small
407 biopsy to substantial quantity. *J. Sci. Food Agric.* **101**, 7–14 (2021).
408 6. Wilks, M., Phillips, C. J. C., Fielding, K. & Hornsey, M. J. Testing potential psychological
409 predictors of attitudes towards cultured meat. *Appetite* **136**, 137–145 (2019).
410 7. Bryant, C. & Barnett, J. Consumer acceptance of cultured meat: A systematic review. *Meat*
411 *Sci.* **143**, 8–17 (2018).
412 8. Mukund, K. & Subramaniam, S. Skeletal muscle: A review of molecular structure and
413 function, in health and disease. *Wiley Interdiscip. Rev. Syst. Biol. Med.* **12**, e1462 (2020).
414 9. Forcina, L., Miano, C., Pelosi, L. & Musarò, A. An Overview about the Biology of Skeletal
415 Muscle Satellite Cells. *Curr. Genomics* **20**, 24–37 (2019).
416 10. Dohmen, R. G. J. *et al.* Muscle-derived fibro-adipogenic progenitor cells for production of
417 cultured bovine adipose tissue. *Npj Sci. Food* **6**, 6 (2022).
418 11. Reiss, J., Robertson, S. & Suzuki, M. Cell Sources for Cultivated Meat: Applications and
419 Considerations throughout the Production Workflow. *Int. J. Mol. Sci.* **22**, 7513 (2021).
420 12. Giordani, L. *et al.* High-Dimensional Single-Cell Cartography Reveals Novel Skeletal
421 Muscle-Resident Cell Populations. *Mol. Cell* **74**, 609-621.e6 (2019).
422 13. De Micheli, A. J., Spector, J. A., Elemento, O. & Cosgrove, B. D. A reference single-cell
423 transcriptomic atlas of human skeletal muscle tissue reveals bifurcated muscle stem cell
424 populations. *Skelet. Muscle* **10**, 19 (2020).
425 14. De Micheli, A. J. *et al.* Single-Cell Analysis of the Muscle Stem Cell Hierarchy Identifies
426 Heterotypic Communication Signals Involved in Skeletal Muscle Regeneration. *Cell Rep.* **30**,
427 3583-3595.e5 (2020).
428 15. Rubenstein, A. B. *et al.* Single-cell transcriptional profiles in human skeletal muscle. *Sci.*
429 *Rep.* **10**, 229 (2020).

430 16. Williams, K., Yokomori, K. & Mortazavi, A. Heterogeneous Skeletal Muscle Cell and
431 Nucleus Populations Identified by Single-Cell and Single-Nucleus Resolution Transcriptome
432 Assays. *Front. Genet.* **13**, (2022).
433 17. Cornelison, D. D. W. Context Matters: In Vivo and In Vitro Influences on Muscle Satellite
434 Cell Activity. *J. Cell. Biochem.* **105**, 663–669 (2008).
435 18. Khodabukus, A., Prabhu, N., Wang, J. & Bursac, N. In Vitro Tissue-Engineered Skeletal
436 Muscle Models for Studying Muscle Physiology and Disease. *Adv. Healthc. Mater.* **7**,
437 e1701498 (2018).
438 19. Cao, J. *et al.* A human cell atlas of fetal gene expression. *Science* **370**, eaba7721
439 (2020).
440 20. Joe, A. W. B. *et al.* Muscle injury activates resident fibro/adipogenic progenitors that
441 facilitate myogenesis. *Nat. Cell Biol.* **12**, 153–163 (2010).
442 21. Proietti, D. *et al.* Activation of skeletal muscle–resident glial cells upon nerve injury. *JCI*
443 *Insight* **6**, e143469.
444 22. Ding, S. *et al.* Maintaining bovine satellite cells stemness through p38 pathway. *Sci.*
445 *Rep.* **8**, 10808 (2018).
446 23. Sherwood, R. I. *et al.* Isolation of Adult Mouse Myogenic Progenitors: Functional
447 Heterogeneity of Cells within and Engrafting Skeletal Muscle. *Cell* **119**, 543–554 (2004).
448 24. Ben-Arye, T. *et al.* Textured soy protein scaffolds enable the generation of three-
449 dimensional bovine skeletal muscle tissue for cell-based meat. *Nat. Food* **1**, 210–220 (2020).
450 25. Wang, X. & Zhou, L. The Many Roles of Macrophages in Skeletal Muscle Injury and
451 Repair. *Front. Cell Dev. Biol.* **10**, (2022).
452 26. Cantini, M. *et al.* Macrophages Regulate Proliferation and Differentiation of Satellite
453 Cells. *Biochem. Biophys. Res. Commun.* **202**, 1688–1696 (1994).
454 27. Rosenblatt, J. D., Lunt, A. I., Parry, D. J. & Partridge, T. A. Culturing satellite cells from
455 living single muscle fiber explants. *In Vitro Cell. Dev. Biol. Anim.* **31**, 773–779 (1995).
456 28. Barczyk, M., Carracedo, S. & Gullberg, D. Integrins. *Cell Tissue Res.* **339**, 269 (2009).
457 29. Gal-Levi, R., Leshem, Y., Aoki, S., Nakamura, T. & Halevy, O. Hepatocyte growth factor
458 plays a dual role in regulating skeletal muscle satellite cell proliferation and differentiation.
459 *Biochim. Biophys. Acta* **1402**, 39–51 (1998).
460 30. González, M. N. *et al.* HGF potentiates extracellular matrix-driven migration of human
461 myoblasts: involvement of matrix metalloproteinases and MAPK/ERK pathway. *Skelet.*
462 *Muscle* **7**, 20 (2017).
463 31. Hubalek, S., Post, M. J. & Moutsatsou, P. Towards resource-efficient and cost-efficient

464 cultured meat. *Curr. Opin. Food Sci.* **47**, 100885 (2022).
465 32. Bellani, C. F. *et al.* Scale-Up Technologies for the Manufacture of Adherent Cells. *Front.*
466 *Nutr.* **7**, (2020).
467 33. Machado, L. *et al.* Tissue damage induces a conserved stress response that initiates
468 quiescent muscle stem cell activation. *Cell Stem Cell* **28**, 1125-1135.e7 (2021).
469 34. Zammit, P. S. *et al.* Muscle satellite cells adopt divergent fates: a mechanism for self-
470 renewal? *J. Cell Biol.* **166**, 347–357 (2004).
471 35. Dell'Orso, S. *et al.* Single cell analysis of adult mouse skeletal muscle stem cells in
472 homeostatic and regenerative conditions. *Dev. Camb. Engl.* **146**, dev174177 (2019).
473 36. Zeng, W. *et al.* Single-nucleus RNA-seq of differentiating human myoblasts reveals the
474 extent of fate heterogeneity. *Nucleic Acids Res.* **44**, e158 (2016).
475 37. Trapnell, C. *et al.* The dynamics and regulators of cell fate decisions are revealed by
476 pseudotemporal ordering of single cells. *Nat. Biotechnol.* **32**, 381–386 (2014).
477 38. Sousa-Victor, P. *et al.* Geriatric muscle stem cells switch reversible quiescence into
478 senescence. *Nature* **506**, 316–321 (2014).
479 39. Carlson, M. E. *et al.* Molecular aging and rejuvenation of human muscle stem cells.
480 *EMBO Mol. Med.* **1**, 381–391 (2009).
481 40. Fiore, D. *et al.* Pharmacological blockage of fibro/adipogenic progenitor expansion and
482 suppression of regenerative fibrogenesis is associated with impaired skeletal muscle
483 regeneration. *Stem Cell Res.* **17**, 161–169 (2016).
484 41. Uezumi, A. *et al.* Fibrosis and adipogenesis originate from a common mesenchymal
485 progenitor in skeletal muscle. *J. Cell Sci.* **124**, 3654–3664 (2011).
486 42. Kolkmann, A., Essen, A., Post, M. & Moutsatsou, P. Development of a Chemically
487 Defined Medium for in vitro Expansion of Primary Bovine Satellite Cells. *Front. Bioeng.*
488 *Biotechnol.* **10**, (2022).
489 43. Kang, H. M. *et al.* Multiplexed droplet single-cell RNA-sequencing using natural genetic
490 variation. *Nat. Biotechnol.* **36**, 89–94 (2018).
491 44. Hafemeister, C. & Satija, R. Normalization and variance stabilization of single-cell RNA-
492 seq data using regularized negative binomial regression. *Genome Biol.* **20**, 296 (2019).
493 45. Hao, Y. *et al.* Integrated analysis of multimodal single-cell data. *Cell* **184**, 3573-3587.e29
494 (2021).
495 46. McInnes, L., Healy, J. & Melville, J. UMAP: Uniform Manifold Approximation and
496 Projection for Dimension Reduction. Preprint at https://doi.org/10.48550/arXiv.1802.03426
497 (2020).

498 47. Stuart, T. *et al.* Comprehensive Integration of Single-Cell Data. *Cell* **177**, 1888-1902.e21
499 (2019).
500 48. Thul, P. J. *et al.* A subcellular map of the human proteome. *Science* **356**, eaal3321
501 (2017).
502 49. Gene Ontology Consortium. The Gene Ontology resource: enriching a GOld mine.
503 *Nucleic Acids Res.* **49**, D325–D334 (2021).
504 50. La Manno, G. *et al.* RNA velocity of single cells. *Nature* **560**, 494–498 (2018).
505 51. Bergen, V., Lange, M., Peidli, S., Wolf, F. A. & Theis, F. J. Generalizing RNA velocity to
506 transient cell states through dynamical modeling. *Nat. Biotechnol.* **38**, 1408–1414 (2020).

Acknowledgements

We would like to thank Latifa Karim, Wouter Coppieters, Alice Mayer and Manon Deckers (GIGA institute, ULiège) for support in the acquisition and analysis of scRNA-seq data, Benjamin Bouchet for advice on immunofluorescent stainings, Christoph Börlin for help with RNA velocity analysis and Dhruv Raina for critical feedback on the manuscript.

Author contributions

TM, RGJD, LS, LM, RH and MG performed experiments and analysis. MJP and JEF supervised the study. TM and JEF wrote the manuscript with input from all authors.

Competing interests

TM, RGJD, LS, LM, RH, MG and JEF are employees of Mosa Meat B.V. MJP is co-founder and stakeholder of Mosa Meat B.V. Study was funded by Mosa Meat B.V. Mosa Meat B.V. has patents on serum-free proliferation medium (WO2021158103A1) and the use of cell-type selective media for cultured/cultivated meat production (pending). All authors declare no other competing interests.

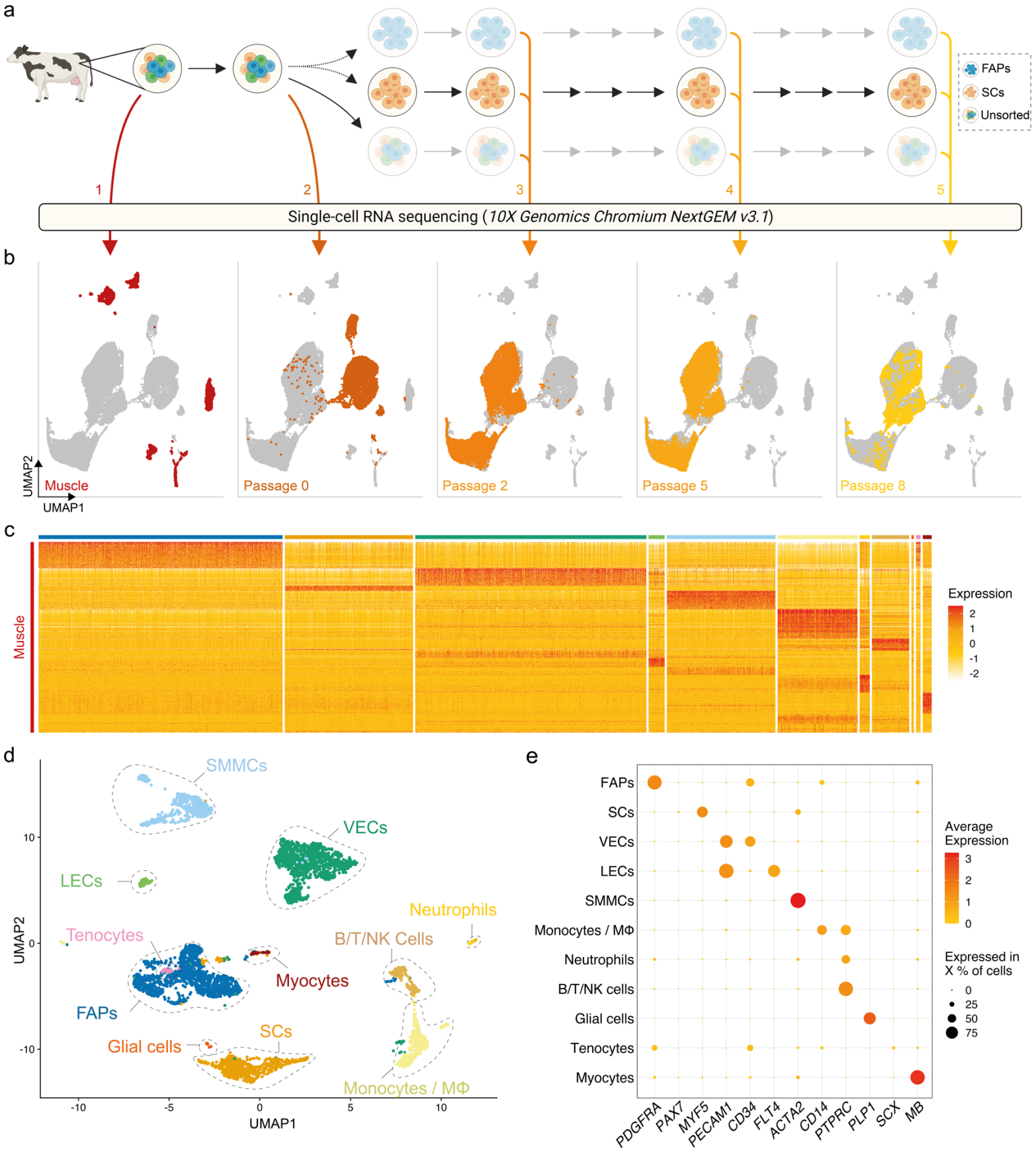
a
FAPs
SCs
Unsorted
1
2
3
4
5
Single-cell RNA sequencing (10X Genomics Chromium NextGEM v3.1)
b
UMAP2
UMAP1
Muscle
Passage 0
Passage 2
Passage 5
Passage 8
c
Muscle
Expression
2
1
0
-1
-2
d
SMMCs
VECs
LECs
Neutrophils
Tenocytes
B/T/NK Cells
Myocytes
FAPs
SCs
Glial cells
Monocytes / MΦ
UMAP2
UMAP1
10
0
-10
-10
-5
0
5
10
e
FAPs
SCs
VECs
LECs
SMMCs
Monocytes / MΦ
Neutrophils
B/T/NK cells
Glial cells
Tenocytes
Myocytes
PDGFRA
PAX7
MYF5
PECAM1
CD34
FLT4
ACTA2
CD14
PTPRC
PLP1
SCX
MB
Average Expression
3
2
1
0
Expressed in X % of cells
0
25
50
75

524 **Figure 1: Single-cell RNA sequencing of bovine muscle and muscle-derived cell**
525 **cultures.**

526 a) Overview of experimental design; coloured arrows and numerals indicate timepoints of
527 RNA sequencing of single cells isolated from bovine muscle (Timepoint 1), at passage 0
528 after 72 h in serum-free growth medium (2) and at passages 2, 5 and 8 (3, 4 and 5
529 respectively); solid arrows indicate passaging, dotted arrows indicate FACS sorting;
530 b) Combined UMAP plots showing single cells (individual points) from all five experimental
531 timepoints; clustering is based on first 30 principal components, cells from each
532 timepoint are coloured in each respective plot;
533 c) Heatmap displaying normalised expression of significantly upregulated genes in each
534 cluster identified in Timepoint 1.
535 d) UMAP of Timepoint 1; cells are coloured and clusters labelled for their assigned cell
536 types;
537 e) Dotplot showing normalised expression of cell-type specific genes, averaged within each
538 population; dot size indicates percentage of cells expressing the respective gene with at
539 least 1 count.

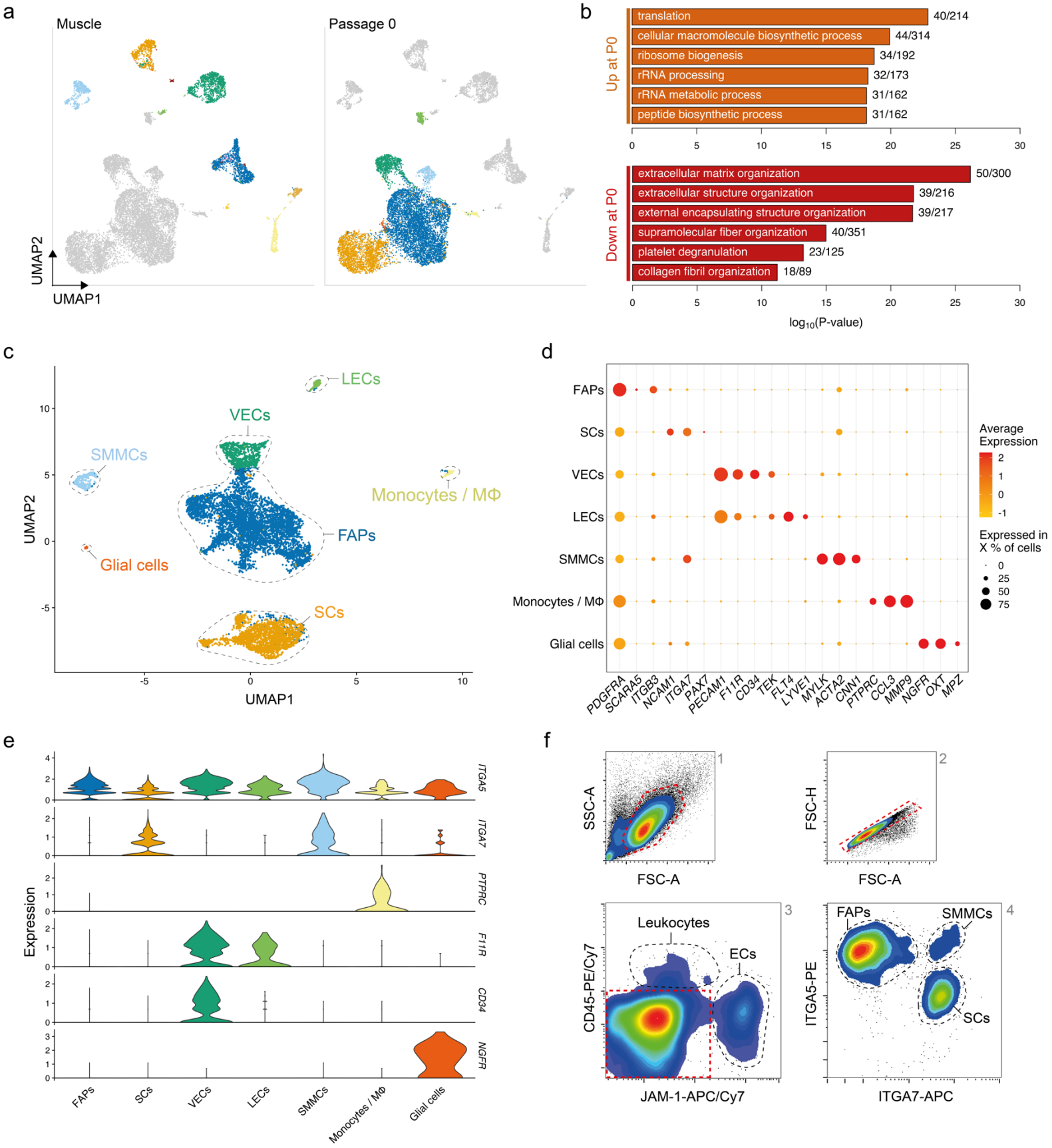
a
Muscle
Passage 0
UMAP2
UMAP1
b
Up at P0
translation 40/214
cellular macromolecule biosynthetic process 44/314
ribosome biogenesis 34/192
rRNA processing 32/173
rRNA metabolic process 31/162
peptide biosynthetic process 31/162
Down at P0
extracellular matrix organization 50/300
extracellular structure organization 39/216
external encapsulating structure organization 39/217
supramolecular fiber organization 40/351
platelet degranulation 23/125
collagen fibril organization 18/89
log10(P-value)
c
LECs
VECs
SMMCs
Monocytes / MΦ
FAPs
Glial cells
SCs
UMAP2
UMAP1
d
FAPs
SCs
VECs
LECs
SMMCs
Monocytes / MΦ
Glial cells
PDGFRA SCARA5 ITGB3 NCAM1 ITGA7 PAX7 PECAM1 F11R CD34 TEK FLT4 LYVE1 MYLK ACTA2 CNN1 PTPRC CCL3 MMP9 NGFR OXT MPZ
Average Expression
Expressed in X % of cells
e
ITGA5
ITGA7
PTPRC
F11R
CD34
NGFR
Expression
FAPs SCs VECs LECs SMMCs Monocytes / MΦ Glial cells
f
SSC-A
FSC-A
FSC-H
CD45-PE/Cy7
JAM-1-APC/Cy7
Leukocytes
ECs
ITGA5-PE
ITGA7-APC
FAPs
SMMCs
SCs

541 **Figure 2: Transcriptomic analysis defines adherent cell types with distinct**
542 **immunosurface phenotypes.**

543 a) Combined UMAP of Timepoints 1 and 2, coloured for populations in Timepoint 1 (left) or
544 2 (right), respectively;
545 b) Top five most significantly enriched GO terms corresponding to differentially expressed
546 genes up- (top) or downregulated (bottom) between Timepoints 1 and 2, after regressing
547 out the effect of cell type;
548 c) UMAP of Timepoint 2; cells are coloured and clusters labelled for their assigned cell
549 types;
550 d) Normalised gene expression of canonical markers in each population at Timepoint 2;
551 e) Violin plots showing expression of surface markers in different cell types at Timepoint 2;
552 f) Representative flow cytometry contour plots showing gating strategy for purification of
553 cell types; red dashed lines indicate gates for the subsequent plot (from 1 to 4); black
554 dashed lines indicate sorting gates for the labelled populations.

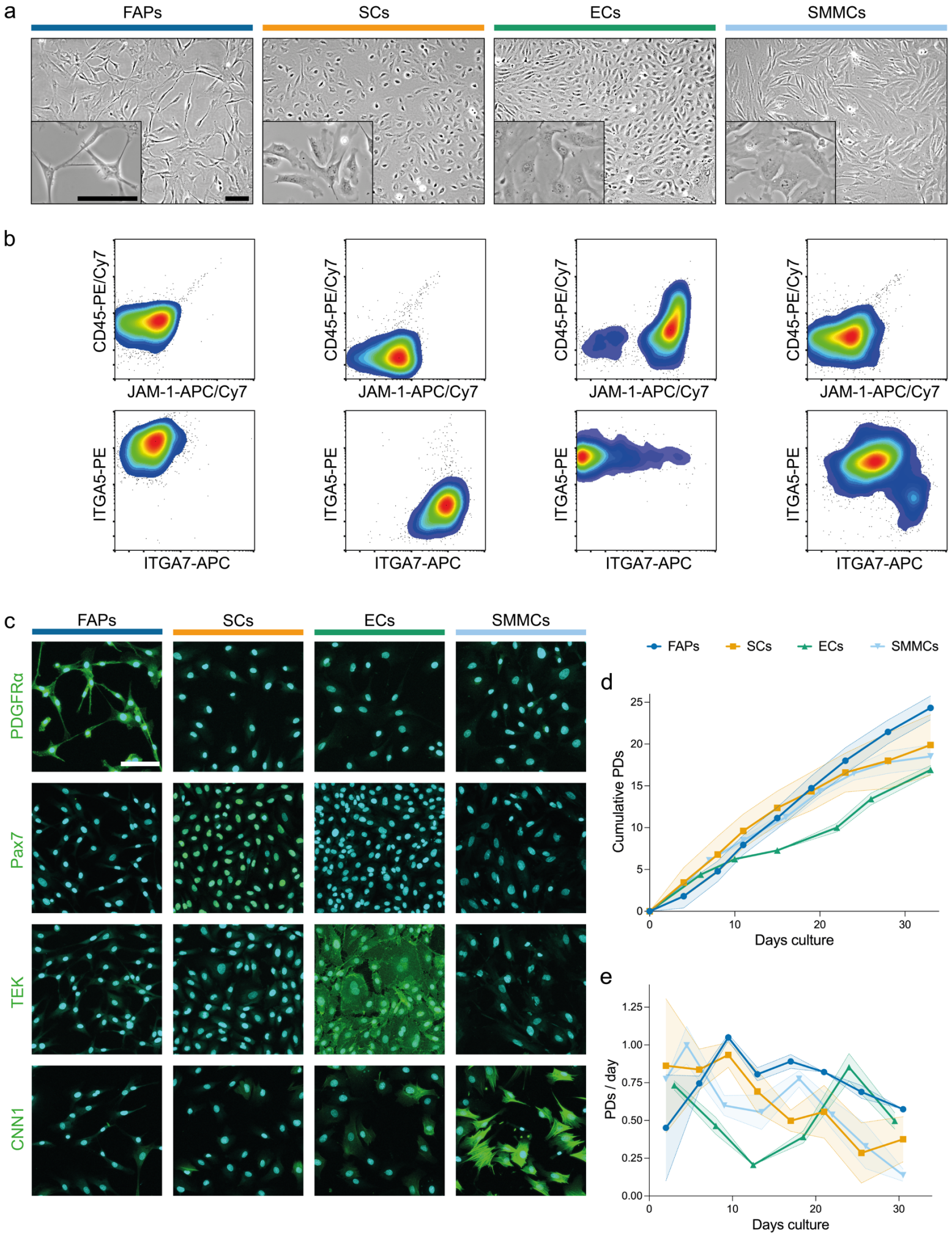
a
FAPs
SCs
ECs
SMMCs
b
CD45-PE/Cy7
JAM-1-APC/Cy7
ITGA5-PE
ITGA7-APC
c
PDGFRα
Pax7
TEK
CNN1
d
Cumulative PDs
Days culture
e
PDs / day
Days culture

556 **Figure 3: Four muscle-derived cell types can be purified and expanded in long-term**
557 **culture.**

558 a) Brightfield microscopy images of purified FAPs (blue), SCs (orange), ECs (green) and
559 SMMCs (light blue) in vitro; scale bars = 100 µm;
560 b) Flow cytometry plots of purified cell types stained for CD45/JAM-1 (top) and
561 ITGA5/ITGA7 (bottom);
562 c) Immunofluorescent staining for PDGFRα, Pax7, TEK and CNN1 (green) in purified cell
563 types; nuclei stained with Hoechst (cyan); scale bar = 100 µm;
564 d) Long-term growth curves of purified cell types in vitro, shown as cumulative population
565 doublings (PDs); shaded areas indicate standard deviation (*SD*), n = 3;
566 e) Growth rates for long-term growth experiments shown in d), shown as PDs per day, n =
567 3.

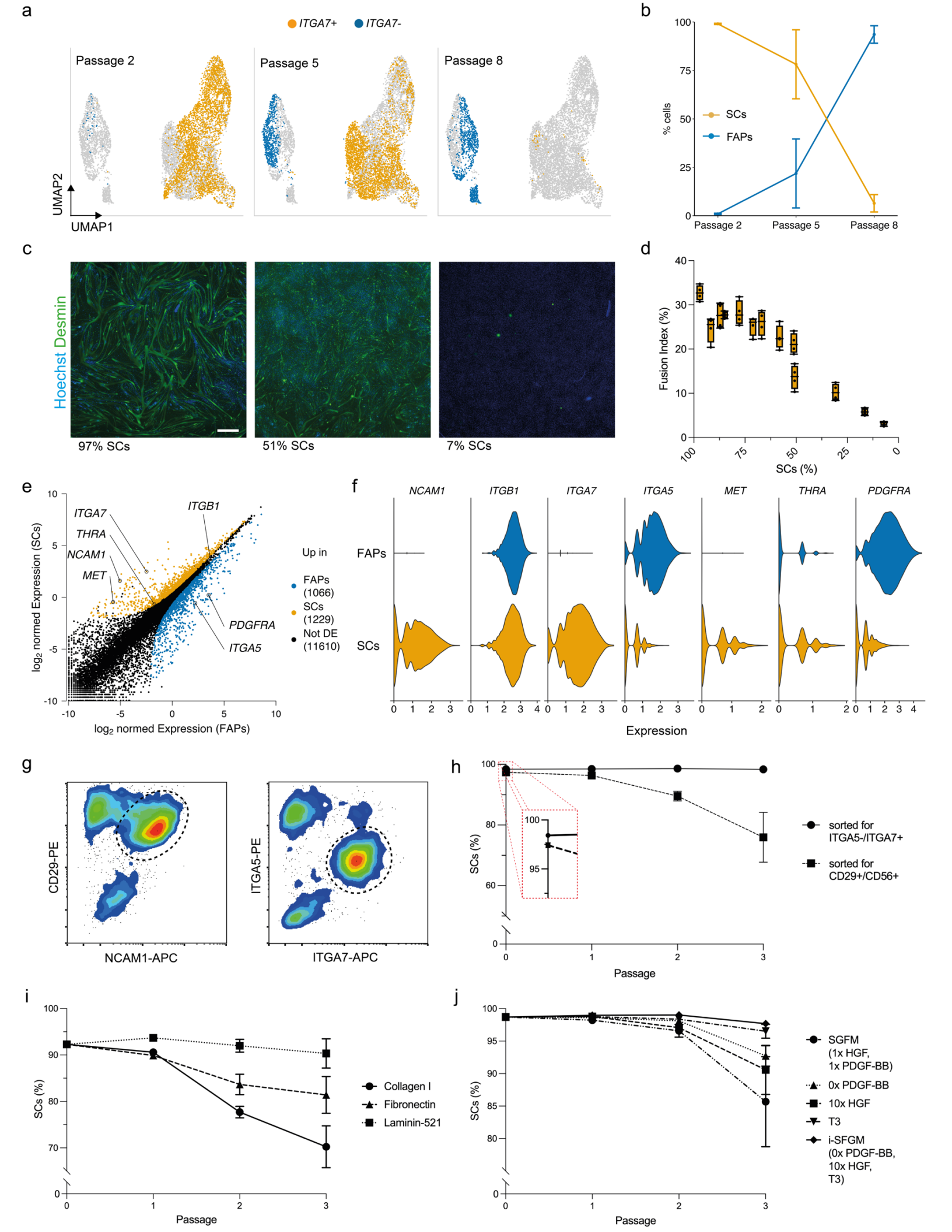
a
ITGA7+
ITGA7-
Passage 2
Passage 5
Passage 8
UMAP2
UMAP1
b
% cells
SCs
FAPs
Passage 2
Passage 5
Passage 8
c
Hoechst Desmin
97% SCs
51% SCs
7% SCs
d
Fusion Index (%)
SCs (%)
e
ITGA7
THRA
NCAM1
MET
ITGB1
PDGFRA
ITGA5
log2 normed Expression (SCs)
log2 normed Expression (FAPs)
Up in
FAPs (1066)
SCs (1229)
Not DE (11610)
f
NCAM1
ITGB1
ITGA7
ITGA5
MET
THRA
PDGFRA
FAPs
SCs
Expression
g
CD29-PE
NCAM1-APC
ITGA5-PE
ITGA7-APC
h
SCs (%)
Passage
sorted for ITGA5-/ITGA7+
sorted for CD29+/CD56+
i
SCs (%)
Passage
Collagen I
Fibronectin
Laminin-521
j
SCs (%)
Passage
SGFM (1x HGF, 1x PDGF-BB)
0x PDGF-BB
10x HGF
T3
i-SFGM (0x PDGF-BB, 10x HGF, T3)

Figure 4: Optimised culture conditions prevent overgrowth of SCs.

a) Combined UMAPs of sorted SCs at passages 2 (Timepoint 3, left), 5 (Timepoint 4, centre) and 8 (Timepoint 5, right); clusters in respective passages are coloured for *ITGA7* expression;
b) Proportion of SCs (*ITGA7*+) during long-term culture; error bars indicate *SD*, n = 3;
c) Immunofluorescent staining of cultures with varying proportions of SCs for desmin (green) and Hoechst (blue) after 72 h in serum-free myogenic differentiation media; scale bar = 100 µm;
d) Fusion indices (nuclei within desmin-stained areas as a proportion of total nuclei) corresponding to c), shown as box plots, n = 4;
e) Normalised gene expression in SCs and FAPs at passage 2 (Timepoint 3). Points represent genes, which are coloured if significantly (FDR < 0.05, log-FC > 1) upregulated in FAPs (blue) or SCs (orange). Selected genes are annotated.
f) Violin plots showing expression of differentially expressed receptors in SCs and FAPs at passage 2;
g) Flow cytometry plots of muscle-derived cells after 72 h in SFGM stained for ITGA5/ITGA7 (left) or CD29/NCAM1 (right) prior to FACS; cells are shown after removal of doublets, CD45+ and JAM-1+ cells; dashed lines indicated gating strategy for sorting;
h) Proportion of SCs purified with FACS protocols shown in g) during long-term culture, as measured by flow cytometry; error bars indicate *SD*, n = 3;
i) Proportion of SCs during long-term culture on different coatings as indicated, n = 3;
j) As i), but for different media formulations as indicated, n = 3.

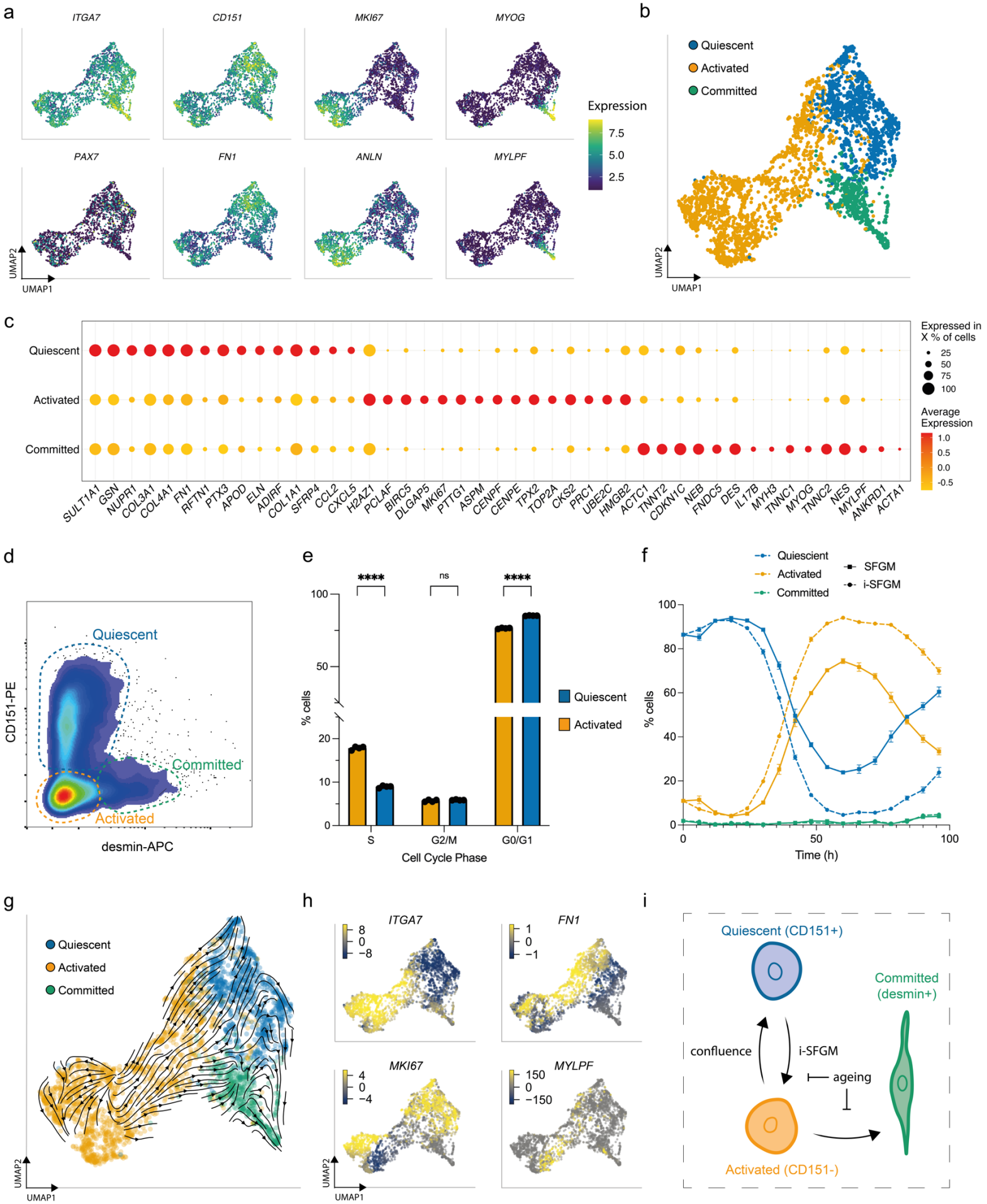
a
ITGA7
CD151
MKI67
MYOG
PAX7
FN1
ANLN
MYLPF
Expression
7.5
5.0
2.5
UMAP2
UMAP1
b
Quiescent
Activated
Committed
UMAP2
UMAP1
c
Quiescent
Activated
Committed
SULT1A1 GSN NUPR1 COL3A1 COL4A1 FN1 RFTN1 PTX3 APOD ELN ADIRF COL1A1 SFRP4 CCL2 CXCL5 H2AZ1 PCLAF BIRC5 DLGAP5 MKI67 PTTG1 ASPM CENPF CENPE TPX2 TOP2A CKS2 PRC1 UBE2C HMGB2 ACTC1 TNNT2 CDKN1C NEB FNDC5 DES IL17B MYH3 TNNC1 MYOG TNNC2 NES MYLPF ANKRD1 ACTA1
Expressed in X % of cells
25
50
75
100
Average Expression
1.0
0.5
0.0
-0.5
d
Quiescent
Committed
Activated
CD151-PE
desmin-APC
e
****
ns
****
% cells
Quiescent
Activated
S
G2/M
G0/G1
Cell Cycle Phase
f
Quiescient
Activated
Committed
SFGM
i-SFGM
% cells
Time (h)
g
Quiescent
Activated
Committed
UMAP2
UMAP1
h
ITGA7
FN1
MKI67
MYLPF
UMAP2
UMAP1
i
Quiescent (CD151+)
Committed (desmin+)
confluence
i-SFGM
ageing
Activated (CD151-)

592 **Figure 5: SCs switch dynamically between three cellular states in vitro.**

593 a) UMAPs of SCs at passage 2 (Timepoint 3), coloured by expression of indicated genes;
594 b) UMAP as a), but labelled according to SC state;
595 c) Normalised expression of the 15 most upregulated genes, averaged within SCs in each
596 state;
597 d) Flow cytometry plot of purified SCs stained for CD151 and desmin; dashed gates
598 indicate the respective cell states;
599 e) Cell cycle analysis of CD151+ (blue) and CD151- cells (orange) determined via flow
600 cytometry using the gating strategy in Supplementary Fig. 5e;
601 f) Proportion of activated, quiescent and committed SCs over one passage in SFGM or i-
602 SFGM media, as determined via flow cytometry;
603 g) UMAP as b), with averaged RNA velocity vectors embedded;
604 h) UMAPs as a), coloured by RNA velocities of denoted genes;
605 i) Dynamic model of SC states in vitro; arrows indicate direction(s) of proposed transitions
606 between states.